Amniotic Fluid-derived Extracellular Vesicles Significantly Improved the Human PC12 Cell Proliferation and Neural Tissue Regeneration

M. Shahlaei, M. Saeidifar* and A. Zamanian

Department of Nanotechnology and Advanced Materials, Materials and Energy Research Centre, Karaj, Iran

ABSTRACT

Extracellular vesicles (EVs) are natural phospholipid molecular biological compounds endogenously secreted by different cell types and suitable to deliver macromolecules such as proteins. They maintain the physiological balance by mediating the intercellular signaling. Meanwhile, their regenerative potential is mainly related to the regulation of cell apoptosis, differentiation, cell proliferation, inflammation, and angiogenesis. The objective of this study was to evaluate the effects of human Amniotic fluid-derived EVs (hAF-EVs) on the proliferation of human PC12 (hPC12) cell lines. The EVs from amniotic fluid origin were isolated *via* differential centrifugation and characterized for morphology and size. Further, the cell proliferation of EVs was examined on the human PC12 cell line at different concentrations (103-1030 nM) in three days. The MTT results revealed that treatment with hAF-EVs significantly improved the *in vitro* cell proliferation. The hAF-EVs improvement of cell proliferation seemed to be mainly dose dependent. The hAF-EVs also upregulated the Nrf2 (nuclear factor erythroid 2-related factor 2) expression and reduced the IL-6 (Interleukin 6) expression. The optimizing volume of hAF-EVs was shown an appropriate treatment possibility in chick embryos with growth retardation.

INTRODUCTION

Neurological disorders present a challenging treatment because of the poor regenerative potential of the central nervous system (CNS). Over the last decades, cell therapy has become a frontline of regenerative medicine; however, poor pieces of evidence of clinical trials have demanded the extreme focus of scientists to develop proper protocols and approaches [1]. For example, the expression of neurotrophic factors can enhance the therapeutic effect through gene therapy as a complementary approach, but unfortunately, there may cause genetic-change-related possible risks. Evidence of stem cell's paracrine effects was a breakthrough in tissue regeneration [2]. For the time, in 2005, Gnecchi *et al.* showed that mesenchymal stem cells (MSCs) medium indicated cytoprotective effects through Akt1 overexpression in cardio-myocytes under hypoxia, as well as diminished myocardial infarction size and enhanced ventricular functions in both *in vitro* and *in vivo*,

respectively [3,4].

Afterward, in many studies stem cell secretions such as extracellular vesicles (EVs) were reported to stimulate morphological development and functional improvement in the treatment of injuries including FHF (Fulminant hepatic failure), nerve disorders, and myocardial infarction [5-8]. The studies around extracellular vesicles (EVs) have confirmed that they are effectively involved in the regeneration of various tissue types and regulation such as immune regulation including T-cell proliferation as well as monocyte differentiation. EVs as a promising therapeutics for tissue and organ regeneration perform a function like their parent cells or are fairly effective during administered *in vivo* and suitable to deliver macromolecules such as proteins [9,10]. Huang *et al.* showed that macrophage-derived EVs are suitable for Baicalin loading to treat ischemic brain injury [11]. Similarly, in a BTBR mice model treated with mesenchymal stem cells (MSCs)-EVs, significant improvement was observed in the repetitive behavior and social interaction [12]. Furthermore, another study determined that EVs-derived two origins, bone

---

marrow mesenchymal stem cell (BMSC) and human placenta mesenchymal stem cell (hPMSC), could be effective for the recovery of function of cerebral apoplexy and regenerate the myelin [13]. In 1934, Bensley and Hoerr first introduced differential centrifugation to obtain mitochondria and nucleus acid in a moderately short time, and nowadays this technique is considered a good method of isolation and purification of cell secretions such as EVs [14-16]. Based on studies on isolation techniques, the EVs that are isolated by the differential centrifugation have a higher protein content and yield [17].

In this study, the differential centrifugation technique was used to isolate the human amniotic fluid-derived EVs, and then the effectiveness of hAF-EVs was examined on the human PC12 cell line. In the final stage, the effect of hAF-EVs was investigated on a 10-day-old chick embryo which was poisoned with sodium valproate. The aim of this study is to check whether hAF-EVs have extreme therapeutics potential to treat neurological disorders in a clinical approach.

MATERIALS AND METHOD

Materials

The hAF (human Amniotic Fluid) and hPC12 Cell line (human pheochromocytoma cells) were purchased from Erfan Hospital and Pasteur Institute of Iran, respectively. PBS (phosphate buffer saline) tablet, Tris(hydroxymethyl) aminomethane buffer, glycine, polyacrylamide, SDS (Sodium dodecylsulfate), DMEM/F-12 (Dulbecco's Modified Eagle Medium/Nutrient Mixture F-12), DMSO (dimethyl sulfoxide), MTT (tetrazolium salt, 3-(4,5-dimethylthiazol-2-yl)-2,5-diphenyltetrazolium bromide), acetone, paraformaldehyde, Acetic acid (glacial), Haematoxylin, Mercuric (II) oxide, Sodium valproate, and other chemicals were obtained from Sigma-Aldrich. The qPCR Primers were designed by STRC (Stem Cell Technology Research Centre, Tehran, Iran).

Method

Isolation of the hAF-EVs. The differential ultracentrifugation refers to multiple consecutive centrifugations that eliminate ingredients other than EVs particles [16,18]. The human Amniotic Fluid was collected

from four healthy pregnant women (Erfan hospital, Tehran, Iran) and then was filtered by filter paper (ashless) to eliminate the contaminations. The protocol method of differential ultracentrifugation generally involves centrifugation of sequential 2-liter amniotic fluid at $3000 \times g$ for 15 min at 4 ℃, followed by $11000 \times g$ for 15 min at 4 ℃, $14000 \times g$ at 4 ℃, and finally, $100,000 \times g$ for 1 h at 4 ℃ to eliminate cell debris, apoptotic body, microvesicles, and isolation of exosomes, respectively. The first stage of centrifugation is the most important because if the cell debris is not eliminated perfectly, their secretion can contaminate the media. Further, determination of time and velocity of centrifugation should be considered due to the rotor's k-factor (clearance factor) as follows (Eqs. (1) and (2)) [16,19]:

$$k = (2.533 \times 10^5 \times \ln(r_{max}/r_{min}))/(RPM/1000)^2 \qquad (1)$$

$$T = k/S \qquad (2)$$

Where r_{max} maximum radius, r_{min} minimum radius, T pelleting time, k the rotor's k-factor and S were sedimentation coefficient, respectively. Thus, to use protocol isolation, the type of rotor (swinging bucket and fixed angle) and RCF (relative centrifugal force) should be noted as the high g-force can damage the structure of the EVs (rupture, aggregation). The type of rotor, the amount of filling of the tubes, velocity, viscosity, and time of centrifugation can affect the purity and yield of isolated EVs [20].

Characterization of hAF-EVs. The chemical bonds in AF-EVs were identified by Fourier Transform Infrared Spectroscopy (FTIR Bruker-dector33). The AF-EVs were blended with KBr, then the infrared absorption spectrum was read at 400-4000 cm⁻¹. The proteins of AF-EVs were separated with different sizes and charges via vertical electrophoresis. Based on the Laemmli method, the SDS-PAGE was prepared with SDS (0.1%) and poly-acrylamide (5-16%). The electrophoretic analysis was carried out at 25 ℃ for 2 h (Tris buffer + glycine, 100-170 V), and then stained with Bio-Rad kit. The size distribution and surface charge of hAF-EVs were determined by Nanoparticle Analyzer (SZ-100z, Horiba) at a 90° angle at 4 ℃, to record the EVs size and surface charge. Also, 200 µl of AF-EVs

was resuspended in 10 ml deionized water and analyzed by DLS (Dynamic Light Scattering). Furthermore, the morphology of AF-EVs was carried out by Scanning Electron Microscopy (Tescan Vega II TS) where the images were confirmed by size distribution results. AF-EVs were prepared through fixing them with 2.5% glutaraldehyde in PBS solution in the incubator for 10 min and washed three times with deionized water.

Cellular and Molecular Studies

MTT assay of hAF-EVs treatment. The hPC12 was seeded in 96-well plates at a density 5,000 cells/well in DMEM/F-12 supplemented with 10% FBS and 1% antibiotics (penicillin + streptomycin) at 37 °C and 10% CO_2. Afterward, the cells' attachment was checked out, and the culture media was replaced twice. The EVs (0.021 mM) was added in media culture at different concentrations (1-10 µl) to each column (200 µl media) and incubated with cells for three days in the dark. Next, the medium was replaced with MTT salt solution and was removed after 1 h at 37 °C. Specifically, 150 µl of DMSO was used to solve the formazan crystals. Then, the microplate reader (Thermo Scientific™) was used for reading the plates at 570 nm. The cell viability was obtained as follows in (Eq. (3)) [21,22]:

$$\text{Cell viability (\%)} = (\text{Absorbance}_{samples}/\text{Absorbance}_{control}) \times 100 \quad (3)$$

Real-time PCR Experiment. For real-time PCR, hPC12s were put in 48-well plates at a density 100,000 cells/well in DMEM/F-12 supplemented with 10% FBS and 1% antibiotics (penicillin + streptomycin) and 10% CO_2 at 37 °C. After cell attachment, the columns (500 µl) were treated by different treatment solutions of hAF-EVs (2.5 µl, 0.021 mM) incubated for 24 h. RNA extraction was carried out using the RNA extraction GenElute kit (Sigma-Aldrich), and after cell lysing, they were filtered and washed. The RNA (1 µg) was transcribed into cDNA by SuperScript II (Invitrogen™). Furthermore, the real-time PCR was performed for expression of Interleukin6 (IL-6) NFE2related factor2 (Nrf2) using SYBR-Green master mix (GenDepot, Barker) and designed primers with sequences in Table 1. The PCR amplifications were performed in 12 µl reactions, 40 cycles of 10 s at 95 °C; and as a reference, β-actin was applied in all PCR analyses. The comparative CT method was used to display the fold changes in the analysis of gene expression data.

Chick Embryo's Models in Developmental Brain Study

Chick embryo's treatment. Three groups (A to C) of fertilized eggs were incubated in the incubator at a suitable humidity (60%), and 37.5 ± 0.4 °C for 10 days. The side of eggs were rotated every 1 h with 50º angle during the hatching phase, with the candling carried out using an LED torch to confirm the formation of embryos. 72 h after hatching, two groups (groups B and C) of eggs were injected with different concentrations (35 µM and 65 µM) of sodium valproate. Group A was considered a negative control group, while group 2 was considered a positive control group to better compare the results. Afterward, on the 10th day, the embryos were extracted from the eggs and their heads were severed from their bodies.

Histopathology study of Chick embryo's brain developmental. The formalin-fixed brains (4%

Table 1. Gene, Primer Sequence, and Melting Temperature (ºC)

Gene	Primer sequence	Melting temperature (ºC)
IL-6 (Interleukin-6)	F-CCAGCTATGAACTCCTTCTC R-AGGAGTTCAGAGG	85.87
NRF2 (Nuclear factor erythroid 2-related factor 2)	F-CTCGCTGGA AAAAGA AGTG R-CCGTCCAGGAGTTCAGAGG	82.74
β-actin	F-CACCAT TGGCAATGAGCGGTTC R-AGGTCTTTGCGGATGTCCACGT	84.08

paraformaldehyde for 6 h) from each embryo were embedded in melted paraffin, then the tissues were cut by microtome (5-10 μm in thickness). Afterward, the samples were prepared for staining with Hematoxylin and Eosin (H&E) for 20 min at 37 °C. At the final step, they were washed three times with deionized water, and examinations were performed using an optical microscope.

Statistical analysis. The one-way ANOVA analysis was performed for between-group differences (mean ± SD). The data of real-time PCR and cell viability with different concentrations of EVs (in three doses) were assumed by Tukey's multiple comparisons test [23]. The t-test analysis was used for the neural cell population in the embryo's brain. In brief, for each experiment, the p-value < 0.05 was considered a significant difference, and all analyses were assumed with GraphPad Prism version 8.4.3.

RESULTS AND DISCUSSION

Characterization of hAF-EVs

The size distribution and morphology of hAF-EVs were determined by Nanoparticle Analyzer and scanning electron microscopy. The size distribution curve (Fig. 1) and SEM image (Fig. 1i) of hAF-EVs revealed good size uniformity (<200 nm, considering the hydrodynamic diameter of hAF-EVs) without cracks and agglomeration; however, the shapes were affected by fixation. The results of surface charge of hAF-EVs indicated stability between threshold agglomeration and the threshold delicate dispersion zone (-14 to -16 mv) [24]. Fortunately, as displayed in the SEM image, the zeta potential did not have a significant effect on agglomeration.

The chemical bands of hAF-EVs were examined by Fourier Transform Infrared Spectroscopy (FTIR) technique. The second derivative absorbance in the mid-infrared region (4000-400 cm^{-1}) was applied for discriminating and recognizing different functional groups present in hAF-Evs (Fig. 2b). The region 3500 to 3000 cm^{-1} is dominated by stretching vibrations of C-H (3391 cm^{-1}), while the region 3000 to 2700 cm^{-1} is characteristic for stretching vibrations of CH_2, -CH_3, and CHO groups. The most important region is 1800-1500 cm^{-1}, which is related to protein bands, wherein 1658 cm^{-1} and 1548 cm^{-1} are specific for amide groups, which are generally due to stretching vibrations of
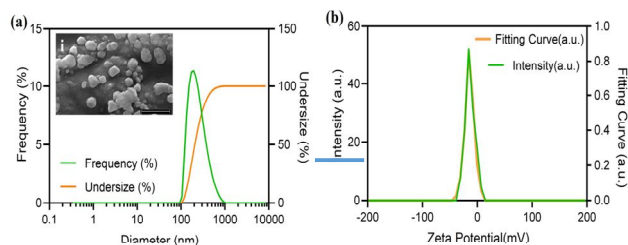
Fig. 1. The characterization of hAF-Evs. (a) Size distribution (Frequency%, and Undersize%), (i) SEM image of hAF-Evs (Scale: 200 nm, 30 Kv) fixed with 2.5% glutaraldehyde at 37 °C for 10 min; (b) Zeta-potential (Intensity, and Fitting curve).
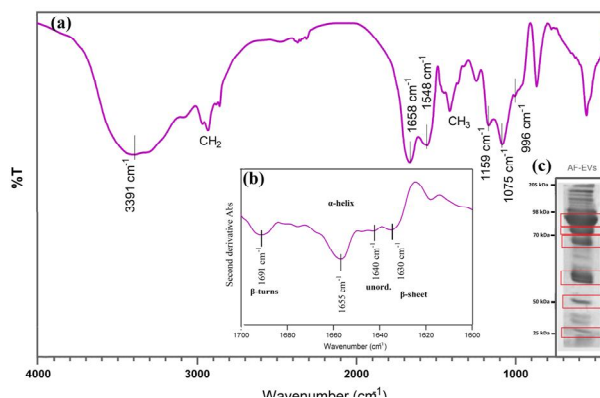
Fig. 2. The composition and structure of hAF-EVs. (a) FTIR spectrum of hAF-EVs (4000-400 cm^{-1}); (b) Second derivative absorbance of hAF-EVs (1700-1600 cm^{-1}); (c) hAF-EVs protein content expression at SDS-PAGE filtration and silver staining.

C=O (peptide band). Thus, the protein bands could be related to the protein content of hAF-EVs. Figure 2b illustrates the β-turn, α-helix, and β-sheet of possible DNA/noncoding and coding RNA content of hAF-Evs [25,26]. In addition, the electrophoretic result of hAF-EVs has shown proteins with 98 to 68,60, 48, as well as 24 KDa molecular weights.

Cellular and Molecular Results

Eventually, we examined whether hAF-EVs can

improve the biological activity of hPC12 cells. To this end, we investigated the different concentrations of hAF-EVs (103 nM, 514.7 nM, 1030 nM) on the hPC12 cell line on day three, after which, the optimized concentration was chosen for the real-time PCR test. The evaluations of the cell viability and gene expression have been illustrated in Fig. 3 that shown the dose 3 has a greater effect on the first and third days. In addition, the maximum cell proliferation is 138% and related to Dose 3 (1030 nM) of hAF-EVs in Day 3 (Fig. 3b). Further, the gene expression shows that the hALF-EVs can strongly activate the Nrf2 signaling pathway. The Nrf2 signaling pathway remains a crucial therapeutic approach for neurological disorder treatment. According to studies on autism, there is a relationship between Nrf2 expression and autism. Under expression of Nrf2 has been reported in the frontal cortex of autistic patients. Furthermore, there are abnormalities in the expression of other genes which are implicated in redox homeostasis. [27]. Many investigations have confirmed that Nrf2 provides the anti-inflammatory process through the organizing recruitment of inflammatory cells and gene expression regulation by the antioxidant response element (ARE). Thus, the identification of Nrf2 signaling pathway activators has become an important key in drug development [28,29]. Although the expression of IL-6 has not been significantly changed; however it can be affected at higher doses or using a suitable drug and loading into hAF-EVs for reaching higher efficiency. Eventually, increasing the cell viability and effective Nrf2 gene regulation led us to confirm that the hAF-EVs can be a good candidate for treatment of autism spectrum disorder (ASD).

Histopathology Study of Chick Embryo's Brain Developmental

Chick embryos are nominated as a substitute to mammalian models because of minimal ethical consideration [30]. The avian embryos have been applied in studies that involve regenerative medicine, pharmacology, cancer research, angiogenesis, allergology, and infectiology [30-32]. In this study, the chick embryos were grown based on different situations such as negative control (normal), positive control (sodium valproate, injection 35 µM for each egg), and treated (100 µl, 0.021 mM). Afterward, their brains were stained using hematoxylin and eosin (H&E).

(a)   **(b)**   **(c)**
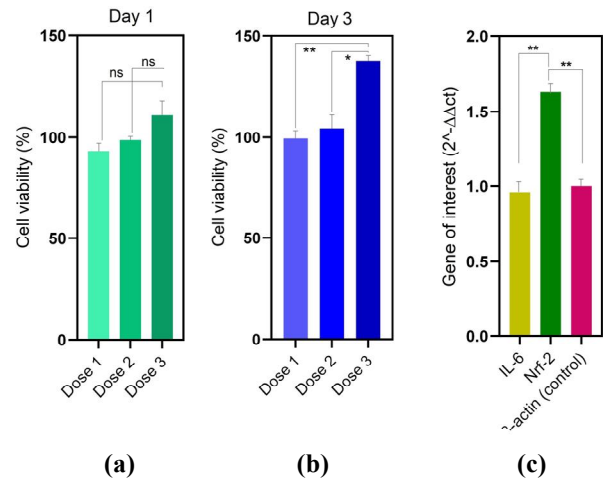
Fig. 3. Cell prolifration after incubation with hAF-EVs. (a) Cell viability (%) of 1-day incubation with hAF-EVs in three Dose (103 nM, 514.7 nM, 1030 nM); (b) Cell viability (%) of 3-day incubation with hAF-EVs in three Dose (103 nM, 514.7 nM, 1030 nM); (c) Gene expression of Nrf2, Il-6, and β-actin (referenc). Data were shown as mean ± SD. $^{ns}p < 0.4$ and $**p < 0.05$ (ANOVA followed by Dunnett's post-hoc test).
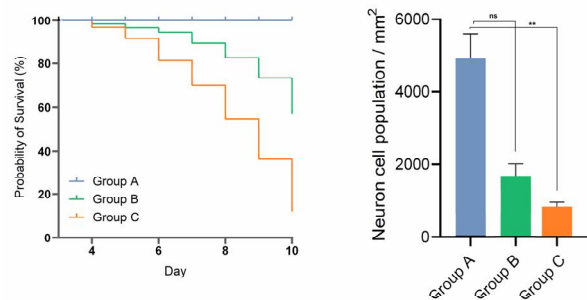
Fig. 4. (a) Kaplan-Meier curve and (b) neuron cell population of Group A-C. Each bar represents the average; (one-way ANOVA, Data were shown as mean ± Std. Deviation), $^{ns}p = 0.57$, $**p < 0.05$.

The Kaplan-Meier curve (Fig. 4a) indicates the number of probability chick embryos' survival of Group A-C. The enormous number of embryos of group C experienced growth retardation and death before the 10th day. However, according to data from Group C, the survival rate decreased after treatment with hAF-EVs. In addition, by comparing

the Kaplan-Meier and neural cell population curves, it can be concluded that hAF-EVs can improve the possibility of treating the neurological disorder. As mentioned earlier in the cellular and molecular results section, it can be affected at higher doses or using a suitable drug and loading into hAF-EVs for reaching higher efficiency.

As seen in the stained coronal brain images, group A is a normal brain of the chick embryo, group B is related to hAF-EVs treatment (100 µl, 0.021 mM), and group C also shows the brain of poisoned animals (sodium valproate, injection 35 µM for each egg) on 10th day. The black thin arrow in Fig. 5a reveals neuronal proliferation, where this stage will be continued until the complete formation of the nervous system to the 13th day [30]. In addition, Fig. 5d indicates the neuronal proliferation while there is no evidence of existence of this area in group C. The images of group C have indicated wide myelin vacuolation within the white matter of chick embryos (due to sodium valproate toxicity) [33]. On the other hand, in group B, the hAF-EVs treatment has had an acceptable effect on neuronal proliferation. In addition, the difference between the coherence of the grey and white matter and the neuron orientation is very noticeable in groups A-B and C.

CONCLUSIONS

The neuropathological study of the effectiveness of hAF-EVs on neurological disorders indicated the treatment possibility. The hAF-EVs can regenerate and repair the neural migration and restore the function of the neurons as with other tissues. Our outcomes also demonstrate that hAF-EVs inhibit the neurological disorder progression by activating the Nrf2 as a neuroprotective pathway since these abnormalities are caused by oxidative stress. The activation of the Nrf2 pathway can protect neurons from oxidative stres. The chick embryo model was chosen for histopathological study; the results indicated a reduction in myelin vacuolation within the white matter, and improved neuronal proliferation, coherence of the grey and white matter, and the neuron orientation. For the future study, we speculate cell viability could be enhanced using higher doses or a suitable drug and incorporation into hAF-EVs for reaching higher efficiency.
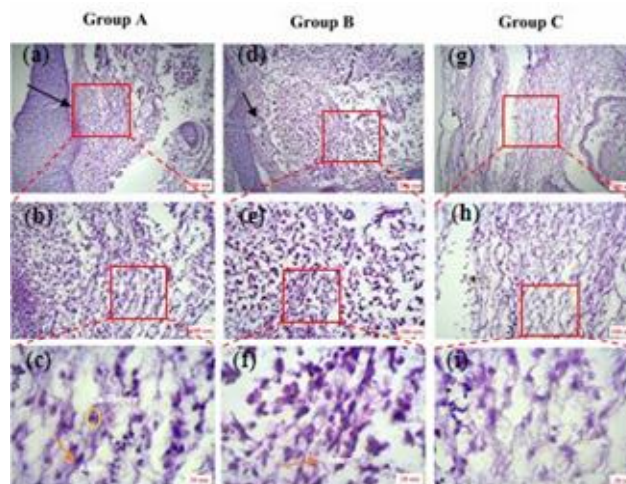
Fig. 5. Coronal cross-section of chick embryos' brain stained by hematoxylin and eosin; H&E images of Group A (a-c) negative control (normal), Group B (d-f) treatment with hAF-EVs, and Group C (g-i) positive control (exposed to sodium valproate). Scale: 200 um, 100 um, and 20 um, respectively; the Axon of bipolar neurons (orange arrow), cell body (yellow circle), and the area of neural proliferation (black arrow) have been marked.

ACKNOWLEDGMENTS

REFERENCES

[1] A.U. Hassan, G. Hassan, Z. Rasool. Int. J. Health Sci. 3 (2009) 227.

[2] L.R. Galieva, V. James, Y.O. Mukhamedshina1, A.A. Rizvano, Front. Neurosci. 13 (2019) 163.

[3] M. Gnecchi, H. He, O.D. Liang, L.G. Melo, H. Mu, N. Noiseux, L. Zhang, R.E. Pratt, J.S. Ingwall, V.J. Dzau, Nat. Med. 11 (2005) 368.

[4] M. Gnecchi, H. He, N. Noiseux, O.D. Liang, L. Zhang, F. Morello, H. Mu, L.G. Melo, R.E. Pratt, J.S. Ingwall, V.J. Dzau, FASEB J. 6 (2006) 669.

[5] B. Parekkadan, D.V. Poll, K. Suganuma, E.A. Carter,

F. Berthiaume, A.W. Tilles, M.L. Yarmush. PloS one. 9 (2007) 941.

[6] L. Timmers, S.K. Lim, F. Arslan, J.S. Armstrong, I.E. Hoefer, P.A. Doevendans, J.J. Piek, R.M. El Oakley, A. Choo, C.N. Lee, P. Kleijn, Stem Cell Res. 8 (2008) 137.

[7] Y. Zhang, M. Chopp, Y. Meng, M. Katakowski, H. Xin, A. Mahmood, Y. Xiong, J. Neurosurg. 122 (2015) 867.

[8] J.L. Williams, N.N. Gatson, K.M. Smith, A. Almad, D.M. McTigue, C.C. Whitacre, Clin. Immunol. 149 (2013) 243.

[9] A. Nagelkerke, M. Ojansivu, L. van der Koog, T.E. Whittaker, E.M. Cunnane, A.M. Silva, N. Dekker, M.M. Stevens, Adv. Drug Deliv. Rev. 175 (2021) 113775.

[10] X. Zhang, Q. Xu, Z. Zi, Z. Liu, C. Wan, L. Crisman, X. Liu, Dev. Cell. 55 (2020) 801.

[11] Z. Huang, L. Guo, L. Huang, Y. Shi, J. Liang, L. Zhao, Mat. Sci. Eng. C 126 (2021) 112123.

[12] N. Perets, S. Hertz, M. London, D. Offen, Mol. Autism. 9 (2018) 57.

[13] K. Clark, S. Zhang, S. Barthe, P. Kumar, C. Pivetti, N. Kreutzberg, C. Reed, Y. Wang, Z. Paxton, D. Farmer, F. Guo, Cells. 8 (2019) 1497.

[14] M.G. Ord, L.A. Stocken (Eds.), 1995.

[15] P.C. Liao, C. Bergamini, R. Fato, L.A. Pon, F. Pallotti, in: L.A. Pon, E.A. Schon (Eds.), 2020.

[16] M.A. Livshits, E. Khomyakova, E.G. Evtushenko, V.N. Lazarev, N.A. Kulemin, S.E. Semina, E.V. Generozov, V.M. Govorun, Sci. Report. 5 (2015) 17319.

[17] L. Antounians, A. Tzanetakis, O. Pellerito, V.D. Catania, A. Sulistyo, L. Montalva, M.J. McVey, A. Zani, Sci. Report. 9 (2019) 1837.

[18] K. Sidhom, P.O. Obi, A. Saleem, Int. J. Mol. Sci. 21 (2020) 6466.

[19] A. Cvjetkovic, J. Lötvall, C. Lässer. J. Extracell. Vesicle. 3 (2014) 23111.

[20] P.S. Bisen, A. Sharma, Introduction to Instrumentation in Life Sciences. Crc Press., 2012.

[21] Y. Tang, Y. Cui, F. Luo, X. Liu, X. Wang, A. Wu, J. Zhao, Z. Tian, L. Wu, Neural. Regen. Res. 7 (2012) 1105.

[22] J. Khodadi, M. Saeidifar, M. Shahlaei, A. Divsalar, P. Sangpour Biomacromol. J. 5 (2019) 112.

[23] P. Miranda-Azpiazu, S. Panagiotou, G. Jose, S. Saha, Sci. Rep. 8 (2018) 10.

[24] P. Bajpai, P. Bajpai (Eds.), Elsevier, 2018.

[25] J. Mihály, R. Deák, I.C. Szigyártó, A. Bóta, T. Beke-Somfai, Z. Varga, Biochim. Biophys. Acta Biomembr. 1859 (2017) 466.

[26] J.S. Cobb, V. Zai-Rose, J.J. Correia, A.V. Janorkar, ACS Omega. 5 (2020) 8413.

[27] M.S. Schrier, Y. Zhang, M.S.Trivedi, R.C. Deth, Biochim, 2021.

[28] MC. Egbujor, S. Saha, B. Buttari, L. Saso, E. Profumo, Expert. Rev. Clin. Pharmacol. 14 (2021) 480.

[29] S.M.U. Ahmed, L. Luo, A. Namani, X.J. Wang, X. Tang, Biochim. Biophys. Acta Mol. Basis Dis. 1863 (2017) 597.

[30] E. Aleksandrowicz, I. Herr, ALTEX. 32 (2015) 147.

[31] D. Slodownik, I. Grinberg, R.M. Spira, Y. Skornik, R.S. Goldstein, Exp. Dermatol. 18 (2009) 413.

[32] D. Ribatti, Exp. Cell Res. 328 (2014)324.

[33] R.H. Garman, Toxicol. Path. 39 (2011) 35.

[34] J.A. Johnson, D.A. Johnson, A.D. Kraft, M.J. Calkins, R.J. Jakel, M.R. Vargas, P.C. Chen, Ann. N.Y. Acad. Sci. 1147 (2008) 61.